JACS
JOURNAL OF THE AMERICAN CHEMICAL SOCIETY
Article
Cite This: J. Am. Chem. Soc. XXXX, XXX, XXX−XXX
pubs.acs.org/JACS

Programmable Nucleic Acid Nanoswitches for the Rapid, Single-Step Detection of Antibodies in Bodily Fluids

Alessandro Porchetta,[†,#] Rudy Ippodrino,[‡,#] Bruna Marini,[‡] Arnaldo Caruso,[§] Francesca Caccuri,[§] and Francesco Ricci*[,†]

[†]Department of Chemistry, University of Rome, Tor Vergata, Via della Ricerca Scientifica, 00133 Rome, Italy

[‡]Ulisse BioMed S.r.l., Area Science Park, 34149 Trieste, Italy

[§]Department of Molecular and Translational Medicine, Section of Microbiology, University of Brescia Medical School, Piazzale Spedali Civili 1, 25123 Brescia, Italy

Supporting Information

ABSTRACT: Antibody detection plays a pivotal role in the diagnosis of pathogens and monitoring the success of vaccine immunization. However, current serology techniques require multiple, time-consuming washing and incubation steps, which limit their applicability in point-of-care (POC) diagnostics and high-throughput assays. We developed here a nucleic acid nanoswitch platform able to instantaneously measure immunoglobulins of type G and E (IgG and IgE) levels directly in blood serum and other bodily fluids. The system couples the advantages of target-binding induced colocalization and nucleic acid conformational-change nanoswitches. Due to the modular nature of the recognition platform, the method can potentially be applied to the detection of any antibody for which an antigen can be conjugated to a nucleic acid strand. In this work we show the sensitive, fast and cost-effective detection of four different antibodies and demonstrate the possible use of this approach for the monitoring of antibody levels in HIV+ patients immunized with AT20 therapeutic vaccine.

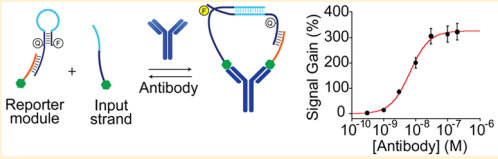

INTRODUCTION

Antibody detection is crucial for the diagnosis of many human disorders including infectious, autoimmune, and oncological diseases.[1,2] Nowadays serological tests for early diagnosis are required to be not only sensitive, quantitative and specific, but also rapid and easy to use. Unfortunately, however, current methods routinely used for this purpose in clinical settings often require reagent-intensive laboratory-based techniques (e.g., ELISA, Western blot assay, radioimmunoassay). In an attempt to find new solutions to this problem several approaches for the fast and sensitive detection of antibodies have been proposed. For example, the most common approach in this rapidly developing area has been to miniaturize state-of-the-art analytical work flows such as immunoassays using microfluidics and lab-on-chip technology.[3−5] Other methods, instead, take advantage of the observation that IgG and IgE antibodies have two identical binding sites separated by about 10−12 nm. Such spatial geometry, that is shared by all IgG and IgE antibodies (i.e., most diagnostically relevant antibodies), has been cleverly used to design and develop novel methods for antibodies detection that are rapid, sensitive and cost-effective.

In this regard several examples have been demonstrated in which a pair of antigen-conjugated signaling probes, upon binding to the two binding sites of the same target antibody, are colocalized in a confined volume. This, in turn, dramatically increases the local concentration of the reporter probes and activates their signaling function.[6,7] For example, Heyduk and co-workers have used FRET-labeled DNA probes that are able to hybridize and generate a FRET signal only when bound to the target antibody.[8,9] Potential drawbacks of the latter strategy include limited signal gains (due to the high background of the free fluorophore in absence of antibody) and nontrivial design issues of the sensing elements. Co-localization of ligands on one antibody has been also employed to allow antibody-induced reconstitution of enzyme activity.[10] However, this approach often fails in reconstituting full enzyme activity thus affecting the sensitivity of the method. To overcome this problem, Merkx and co-workers[11] introduced antibody-based disruption of an enzyme−inhibitor complex; a system that while showing enhanced sensitivity might be difficult to multiplex.

Recently, we and others have employed antigen-conjugated switching probes rationally designed to undergo a conformational change upon binding to a specific target antibody that ultimately leads to a change in signal (either optical or electrochemical).[12−18] In one of these formats we have designed a DNA nanoswitch conjugated with two identical antigens and a fluorophore/quencher signaling pair.[19] When the target antibody binds to each of the two antigens, a conformational change occurs leading to an increase in fluorescence signal. In order to function properly, however, a careful adjustment of the distance between the two identical

Received: September 1, 2017

© XXXX American Chemical Society

DOI: 10.1021/jacs.7b09347
J. Am. Chem. Soc. XXXX, XXX, XXX−XXX

antigens is critical but difficult to achieve especially for larger antigens.

In order to improve upon the above approaches we show here the rational design of programmable nucleic acid nanoswitches for the rapid, single-step detection of antibodies in bodily fluids. The approach we propose couples the advantageous features of DNA-based conformational switching probes (nanoswitches) with those of colocalization based methods but allows to overcome the practical limitations affecting the above-described platforms.

■ RESULTS AND DISCUSSION

Sensing Principle of Programmable DNA-Based Nanoswitches. Our strategy to achieve a programmable nucleic acid nanoswitch for the rapid, single-step detection of antibodies is based on the use of a set of three DNA-based elements that are rationally designed to give a measurable signal in the presence of a specific target antibody. The first element (strand #1, Figure 1, left) is a synthetic DNA sequence

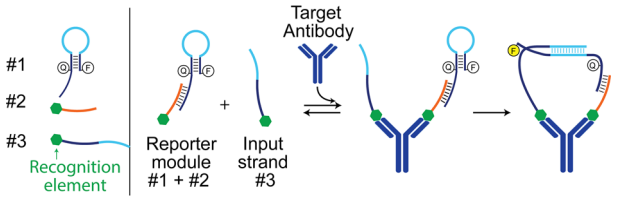

Figure 1. Programmable nucleic acid nanoswitches activated by antibody induced colocalization. The nanoswitch is composed of three synthetic nucleic acid strands. A first DNA strand (strand #1) is a fluorophore/quencher-modified DNA stem-loop flanked by a 15-base single-stranded tail. To create an antibody-reporter module, this tail is hybridized with a second synthetic DNA strand (strand #2) conjugated to an appropriate recognition element (i.e., an antigen, green hexagons). The third element (strand #3, input strand) is a DNA strand conjugated with another copy of the recognition element and contains a portion complementary to the loop sequence of strand #1. In the presence of the target antibody the reporter module (strand #1 + strand #2) and the input strand (strand #3) are colocalized in a confined volume. This brings the stem-loop of strand #1 and the input strand #3 into close proximity, thereby increasing their local concentrations and allowing their efficient hybridization.

designed with two self-complementary portions that lead to a stem-loop conformation flanked by a 15-base DNA tail. Strand #1 is also modified at the two ends of the stem portion with a fluorophore/quencher pair responsible for signaling. The second element (strand #2, Figure 1, left) is a synthetic DNA strand that is conjugated to one copy of an antigen (i.e., the recognition element indicated by the green hexagon in Figure 1, left) and contains a 15-base sequence (orange portion in Figure 1, left) complementary to the tail of strand #1 which allows efficient coupling with it. The third element (strand #3, input strand, Figure 1, left) is conjugated with another copy of the antigen and contains a domain complementary to the loop sequence of strand #1 (blue portion) flanked by a 15-base poly-T linker portion. Of note, strands #1 and #3 are designed so that their binding affinity, in the absence of the target antibody, is poor. Binding of the antibody to the antigens of strand #2 and #3 brings the loop of strand #1 and its cognate portion of strand #3 into close proximity, thereby dramatically increasing their local concentrations (Figure 1, right). This allows efficient binding between strand #1 and strand #3 leading to an increase of the observed fluorescence signal.

Programmable DNA-Based Nanoswitches for Anti-DNP Antibodies Detection. In order to achieve proof of principle of the method, we initially used the small molecule 2,3-dinitrophenol (DNP) as recognition element (i.e., antigen) and an anti-DNP IgE antibody as the target analyte (Figure 2a).

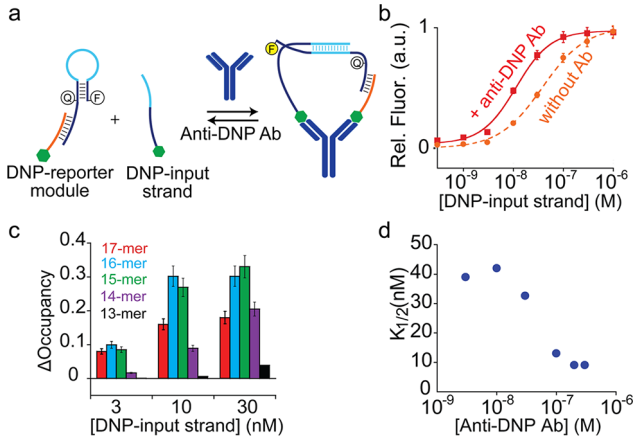

Figure 2. Programmable DNA-based nanoswitches for Anti-DNP antibody detection. (a) As proof-of-principle model we used 2,3-dinitrophenol (DNP) as the recognition element and anti-DNP as target antibody. (b) Binding affinity testing between DNP-reporter module (strand #1 + strand #2, 10 nM) and its complementary 15-base DNA-input strand (strand #3) in the absence (orange) and in the presence (red) of a saturating concentration of anti-DNP antibody (i.e., 100 nM). (c) Antibody-induced difference in occupancy at three different concentrations (i.e., 3, 10, and 30 nM) of strand #3 of different lengths (i.e., from 13 to 17 bases) and at fixed concentrations of reporter module (strands #1 + #2, 10 nM) in the presence and absence of Anti-DNP antibody (100 nM). (d) $K_{1/2}$ (input strand concentration at which we observe half the maximum signal change) values for the binding between the DNP-reporter module (10 nM) and the DNP-input strand as a function of a fixed concentration of anti-DNP antibody in solution. Each value is the average of three determinations ± the standard deviation. The experiments have been performed at 35 °C, in a 100 μL solution of Na_2HPO_4 (50 mM) and NaCl (150 mM) at pH 7.0 with the DNP-reporter module, input strand and anti-DNP antibody at the indicated concentrations.

We designed strand #1 with a highly stable 5-base stem containing 4 GC and 1 AT base pairs and a 15-base loop. Such DNA stem-loop structure is stable from 25 to 35 °C, making the system suitable for clinical applications (Figure S1). This design prevents any significant unwanted annealing reactions with strand #3 in the absence of the target antibody. To achieve optimal sensitivity for antibody detection, we tested different lengths of the complementary domain of strand #3 to the strand #1 loop (ranging from 13 to 17 bases). As expected, binding curves performed at a fixed equimolar concentration of strand #1 and #2 (leading to the reporter module, see Figure 1) combined with increasing concentrations of strand #3 (input strand) showed different affinities with a length-dependent fashion (Figure S2). In the presence of a saturating concentration of the target antibody (i.e., 100 nM) we observed an improvement of the binding affinity with all the tested sequences (Figure 2b and Figure S3). The lengths of complementary portion of strand #3 that lead to the largest change in affinity are 15 and 16 bases (Figure 2c). We selected for further experiments the 15-base long strand #3 to prevent any spurious unwanted hybridization due to minimal changes of the experimental conditions (i.e., ionic strength, pH, etc.),

DOI: 10.1021/jacs.7b09347
J. Am. Chem. Soc. XXXX, XXX, XXX−XXX

which might occur when using real samples. Using this input strand we observed a concentration-dependent change of binding affinity between the DNP-reporter module and DNP-input strand induced by the presence of the anti-DNP antibody (Figure 2d).

The above characterization allowed us to select the optimal concentration of reporter module (i.e., 10 nM) and input strand (i.e., 10 nM) for antibody detection. Under such experimental conditions our platform responds rapidly to anti-DNP antibodies generating a 300-fold increase in fluorescence at saturating concentration of anti-DNP antibodies within 2 min (Figure 3a) and achieving sensitivities in the low

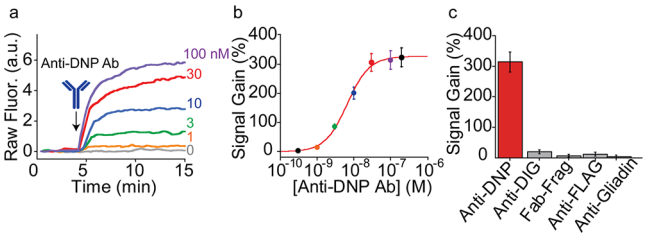

Figure 3. Anti-DNP antibody detection based on DNA nanoswitch activation triggered by colocalization. (a) Kinetic experiments performed through the addition of different concentrations of anti-DNP antibody in solution. (b) Signal gain as a function of antibody concentration ($K_{1/2}$ = 8 ± 4 nM). (c) Determination of the nanoswitch specificity comparing target with negative controls (i.e., 100 nM). The experiments here were conducted at 35 °C in a 100 μL solution of Na_2HPO_4 (50 mM) and NaCl (150 mM) at pH 7.0 containing the DNP-reporter module (10 nM) and the input strand (10 nM) and by adding increasing concentration of anti-DNP antibody.

nanomolar range ($K_{1/2}$ = 8 ± 4 nM; Figure 3b). Notably, because the signal is due to the binding of the antibody to the two recognition elements the platform is highly specific and no significant signal change occurs in the presence of nonspecific antibodies (i.e., 100 nM) (Figure 3c). The platform can be also deployed to detect free antigen (i.e., DNP) in solution in a single-step competitive homogeneous format (Figure S4). Control experiments carried out in the absence of strand #2 or strand #3 further support the proposed sensing mechanism (Figure S5 and SI6). Experiments with different lengths (poly-T of 3 and 40 bases) of the linker portion of strand #3 (see Figure 1) serve as another supports to our sensing principle mechanism. A very short linker (3 bases) does not allow efficient binding of the input strand to the reporter module, likely due to the fact that its length is insufficient to cover the 12 nm distance between the two antibody binding sites (Figure S7). Similarly, a much longer linker (40 bases) while providing sufficient length also provides a higher conformational freedom that ultimately affects the colocalization effect and thus signaling (Figure S7).

One of the major advantages of our sensing mechanism is that it is versatile: changing the recognition elements allows us to potentially detect any class of target antibodies and antigens. To demonstrate this we have employed a different recognition element (i.e., digoxigenin, DIG) and conjugated it to strand #2 and #3. With this new set of sequences we have measured anti-DIG antibodies (IgG) reaching sensitivity and specificity similar to those observed for the anti-DNP antibody (Figure S8). This demonstrates that the approach is flexible and versatile and, because all IgG and IgE antibodies share the same y-shape geometry that supports the proposed detection mechanism, potentially adaptable to the detection of other antibodies.

Modular Programmable DNA Nanoswitches for Antibodies Detection. To further demonstrate the possible utility of our platform for diagnostic applications we then decided to move to more complex antigens. Peptides are by far the most representative class of antigens for diagnostic antibodies. The attachment of peptides to DNA sequences is, however, expensive and challenging from a synthetic point of view,[20−22] two factors that would affect the potential application of our platform for diagnostic use. Motivated by the above considerations we have thus designed a modular version of the above-described platform that would still require a total of 3 oligonucleotides but where only one of them is labeled with the antigen. Such antigen-conjugated strand (strand #2 in Figure 4a) acts as a scaffold to bind both the

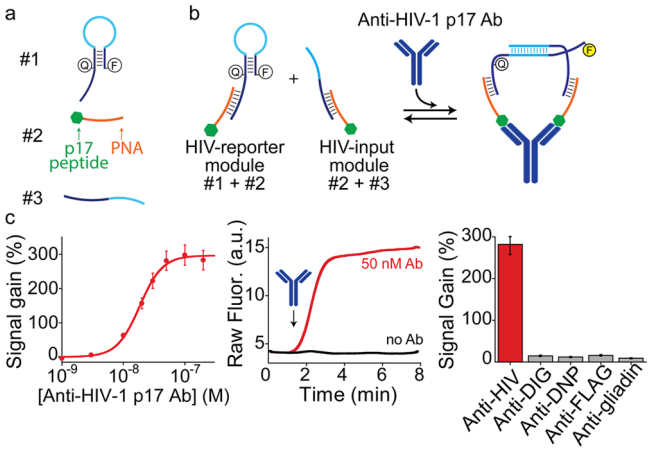

Figure 4. Modular sensing platform for the detection of anti-HIV-1 p17 antibodies. (a) We used a PNA-peptide chimera (strand #2) as the strand responsible for the binding to strand #1 and strand #3. Such PNA-peptide chimera presents a specific HIV-1-p17 epitope (p17) as recognition element. (b) The PNA-peptide chimera allows the HIV-reporter module (#1 + #2) and the HIV-input module (#2 + #3) to be into close proximity only in the presence of the target antibodies against p17 epitope, leading to an increase of the observed fluorescence signal. (c) The modular approach detects anti-HIV-1 p17 antibodies at low nanomolar concentrations ($K_{1/2}$ = 20 ± 4 nM, left). Fluorescence kinetics show that the detection is very rapid, achieving 90% of the fluorescence signal change after less than 3 min (middle); the modular sensor is highly specific and it does not exhibit any significant response in the presence of off-target antibodies (i.e., 100 nM, right). The experiments have been performed at 35 °C in a 100 μL solution of Na_2HPO_4 (50 mM) and NaCl (150 mM) at pH 7.0 containing the HIV-reporter and input modules (strand #1, 20 nM; strand #2, 40 nM; strand #3, 20 nM) at different concentrations of anti-HIV-1 p17 antibodies. Specificity test gives the signal gains obtained under the above experimental conditions and by adding saturating concentrations (i.e., 100 nM) of the anti-HIV-1 antibody and other nonspecific antibodies (all IgG and IgE antibodies).

stem-loop reporter strand and the input strand (i.e., strand #3) (Figure 4b). In this case the antigen-conjugated strand is made of peptide-nucleic acid (PNA), a DNA mimic that, while still maintaining a high sequence specificity toward DNA complementary strands, has a pseudopeptide backbone that makes the conjugation with peptides easier.[23] The modular nature of such approach renders it easily applicable to the detection of different antibodies through the simple expedient of changing only the strand #2 (antigen-conjugated strand).

DOI: 10.1021/jacs.7b09347
J. Am. Chem. Soc. XXXX, XXX, XXX−XXX

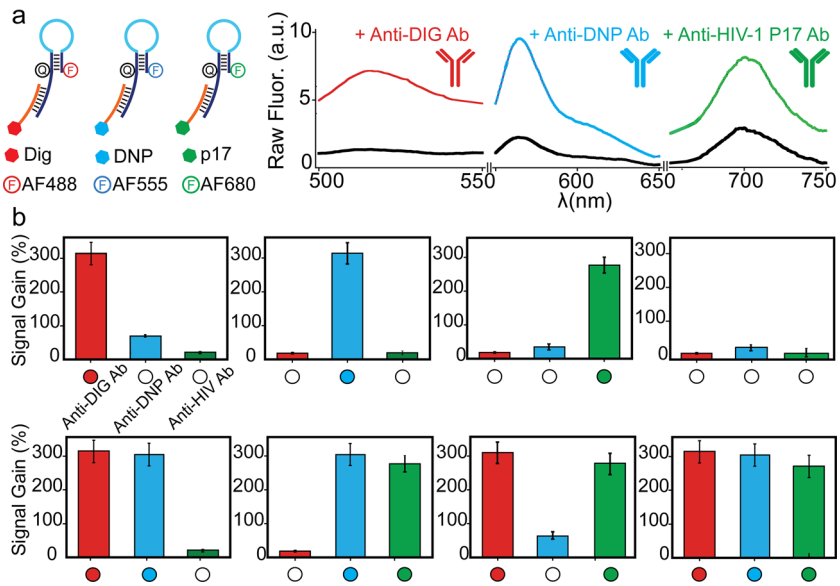

Figure 5. Orthogonal multiplex antibody detection using programmable DNA nanoswitches. (a) Schematics of three reporter modules for the simultaneous multiplex detection of anti-DIG, anti-DNP and anti-HIV-1 p17 antibodies (left). Fluorescence emission spectra measurement in presence and absence of the three target antibodies (i.e., 50 nM). Each reporter module contains its specific input module that can be independently activated in the presence of its cognate antibody (right). (b) Signal gain of the three nanoswitches obtained by adding each antibody in different combinations. Filled and blank circles are used to identify the antibody added in solution. Error bars represent the standard deviation from at least three replicates. The experiments were performed at 35 °C in a 100 μL solution of Na_2HPO_4 (50 mM) and NaCl (150 mM) at pH 7.0 containing the three different nanoswitches (each with the same reporter module and input module/strand concentration reported in Figures 3 and 4).

With this new *modular* and versatile approach we have first employed as recognition element a 12-residue long HIV-1-p17 epitope (p17) recognizing the anti-HIV-1 p17 antibody (Figure 4b). This modular platform results to be equally sensitive, rapid and specific (Figure 4c) as the nonmodular version shown above (Figures 2 and 3). The anti-HIV-1 p17 targeting antibody sensors likewise exhibits similar signal gains (between 260% and 300%), suggesting that the larger antigens employed here do not affect the interaction between the reporter module and the input module. The high specificity of the sensor and its high signal gain due to the binding-induced conformational change of the reporter module in the presence of the anti-HIV1 p17 antibody, renders our sensors selective and sensitive enough to be deployed in complex samples. Our anti-HIV-1 p17 antibody sensor performs well when used in 90% blood serum, producing a $K_{1/2}$ value (i.e., 24 ± 8 nM) comparable to that obtained in phosphate buffer (i.e., 20 ± 4 nM) (Figure S9) and the platform does not show any sign of degradation in this matrix over the time scale of the experiments (Figure S10). We note, however, that the gain observed in blood serum is significantly lower probably due to the higher background fluorescence of this sample matrix.

To further explore the potential of our platform we have tested the possibility of multiplex measurement using the same nanoswitches demonstrated above for the detection of different antibodies (i.e., Anti-DNP, Anti-DIG and Anti-p17 antibodies) and each labeled with a different fluorophore/quencher pairs having distinguishable wavelengths of fluorescence emission. The results demonstrate that we are able to simultaneously detect the three target antibodies in the same solution in an orthogonal way, with signal gains and response times that are not affected by the presence of the other switches (Figure 5).

Detection of Anti-AT20 Antibodies in Human Blood Plasma of Vaccinated Patients. A clinically relevant application of our platform is the monitoring of the immune response elicited from patients that are immunized with a peptide-based therapeutic HIV vaccine. Historically, successful vaccines have been prepared from live attenuated bacteria or viruses or inactivated viruses. In recent years, significant progress has been made to enable a more mechanistic approach to vaccine research and development compared with the traditional empirical approaches.[24] The use of peptides as minimal pathogen components able to stimulate long lasting protection is becoming a pivotal strategy in vaccine development.[25] In this context, peptide-based vaccination represents a promising approach to treat HIV-1 infected patients by boosting or redirecting immune system to neutralize critical HIV-1 antigens whose biological effects are relevant in the context of viral pathogenesis.[26] On the basis of this evidence and successful preclinical data,[27,28] a 20 amino acid synthetic peptide (AT20) representative of the p17 functional region, coupled to the carrier protein keyhole limpet hemocyanin (KLH) was selected as the active agent to perform a therapeutic phase I clinical trial in highly active antiretroviral therapy (HAART)-treated HIV-1-infected patients. While during the natural course of HIV-1 infection the occurrence of an antibody response to AT20 is rare or at very low titer,[29] it was demonstrated that all vaccinated patients developed high titers of high-avidity anti-AT20 antibodies.[27]

Our sensing strategy thus appears potentially useful for monitoring the immune response (i.e., anti-AT20 antibodies titers) of patients which have been subjected to AT20-based HIV-vaccination. Specifically, we used a new PNA-peptide chimera as strand #2 in which the specific AT20 peptide is employed as the recognition element. We first tested our platform using anti-AT20 targeting antibodies. Such anti-AT20 monoclonal antibodies have been developed following immunization of Balb/c mice with AT20 and have been already used as positive controls in competition ELISA assays.[26] Our platform is, once again, able to detect the target antibody

DOI: 10.1021/jacs.7b09347
J. Am. Chem. Soc. XXXX, XXX, XXX−XXX

in a rapid and highly sensitive fashion in a 10% blood plasma (see Figure 6a,b). Of note, titration of the anti-HIV-1 p17

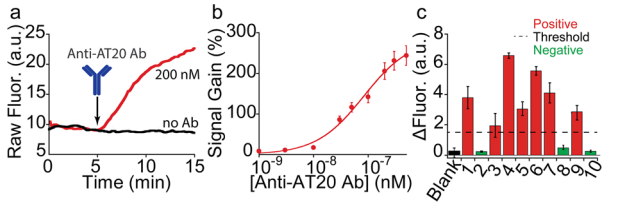

Figure 6. Detection of Anti-AT20 antibodies in human blood plasma from vaccinated individuals. (a) Fluorescence kinetics experiments show that the detection of anti-AT20 antibodies is rapid. (b) The modular sensor detects anti-AT20 antibodies at nanomolar concentrations in 10% human blood plasma ($K_{1/2}$ = 80 ± 10 nM). (c) Anti-AT20 antibodies detection in 10% blood plasma samples of different HIV-positive patients (numbered from 1 to 10) as a way to monitor the immune response induced by the AT-20 vaccine treatment. Seven HIV-positive patients that received the AT20-based HIV-vaccine were easily identified as positive (positive, orange); HIV-positive, non-vaccinated patients tested negative (negative, green). Three different blank blood plasmas were used as negative controls. Threshold value was calculated as the fluorescence signal corresponding to the mean fluorescence signal obtained with three different blank samples of HIV-negative patients +3 times the standard deviation. Binding curve in panel A was carried out at 35 °C in a 100 μL solution obtained by mixing 10 μL of blank blood plasma with 90 μL of Na_2HPO_4 (50 mM) and NaCl (150 mM) at pH 7.0 containing the AT20-reporter and input modules (strand #1, 20 nM; strand #2, 40 nM; strand #3, 20 nM) and different concentrations of anti-AT20 antibodies. To detect the presence of anti-AT20 antibodies in blood plasma sample of HIV-infected patients, 90 μL of the above buffer solution containing the AT20-reporter and the input module was added to 10 μL of the blood plasma sample and the fluorescence signal measured after 10 min.

sensor with anti-AT20 monoclonal antibodies demonstrates that, as expected, the p17 antigen is not able to detect anti-AT20 antibodies (Figure S11). We also note that the platform is quite stable over the time course of the experiment in 10% plasma (Figure S10). We then used our sensor to monitor the long-lasting immune response in HIV-1-infected patients enrolled in a medical trial and vaccinated with the synthetic AT20 peptide. As previously described, HIV-infected patients did not show consistent levels of anti-AT20 antibodies whereas 100% of immunized subjects developed high titers of AT20-specific antibodies.[27] We tested our sensor on samples collected by ten HIV-infected patients, seven of them vaccinated with AT20-KLH. Fluorescence measurements demonstrate that our nucleic acid nanoswitch is able to detect the presence of anti-AT20 antibodies with high specificity in 10% human blood plasma solution of HIV-infected patients. Moreover, our single step fluorescence experiment allows to discriminate in less than 10 min between HIV-infected patients which are under AT20-based vaccine treatments and HIV-infected patients not involved in the treatments (Figure 6c). The same plasma samples were also tested using a control ELISA assay giving comparable results in terms of positive/negative discrimination (Figure S12).

■ CONCLUSION

As in the case of ligand-induced dimerization of cellular receptors that trigger a downstream cascade, we have been inspired to design and develop a new, highly versatile sensing platform that allows detection of clinically relevant IgG and IgE antibodies in complex matrices such as blood serum and plasma in few minutes and without washing steps. We designed fluorescence-based DNA-PNA nanoswitches with low background in the absence of the target antibody. The presence of the target antibody induces an increase of the probes local concentration which ultimately triggers their hybridization. The fluorescence signal generated by the binding-induced conformational change of the DNA-PNA probes system has been used to quantify target antibodies concentration in complex biological matrices.

We demonstrated that our platform can efficiently detect four different antibodies with high sensitivity (low nanomolar levels), excellent specificity (no significant cross-reactivity has been observed) and rapid response time (less than 5 min). Our experiments have shown that the platform is able to efficiently detect antibodies even in complex biological matrices, such as blood serum and blood plasma. We also demonstrated that our method can be used for the simultaneous analysis of multiple antibody targets in the same solution.

Finally, we proposed a clinically relevant application of our method monitoring the immune response of HIV-positive patients enrolled in a medical trial and treated with a peptide-based (AT20 peptide) phase-I therapeutic vaccine. Specifically, we were able to discriminate between AT20-positive subjects (vaccinated patients) and controls (unvaccinated patients). Our nanoswitch-based platform can thus be conveniently used in AT20 Phase II/III clinical trials allowing an extensive and cost-effective monitoring of serological response, whereas the classic ELISA/RIA approach might limit or restrict the analysis to fewer time-points due to costs and time that characterize these assays.

In conclusion we note that, while our direct system, as most of the approaches that do not rely on any amplification step, could not reach the sensitivity of ELISA/RIA methods, it presents features that make it highly advantageous in clinical applications. Apart from the rapid response and high specificity discussed above, the approach is also extremely versatile and can in principle be easily adapted to the detection of any antibody, antigen and bivalent macromolecular targets provided that the relevant recognition element can be coupled to a nucleic acid strand. The method also offers the possibility of multiplexing and, given that it is less reagent-intensive, is inexpensive. For example, a cost of about $0.01/sample, which is approximately 1 order of magnitude lower than that of ELISA assays, can be estimated for the Anti-AT20 antibodies detection platform. The same sensing principle could also be adapted to other output signals (i.e., electrochemical or UV−vis), thus making the platform even more suitable for point-of-care applications and large-scale analysis.

■ EXPERIMENTAL SECTION

Reagents and Materials. All chemicals were of analytical grade and were purchased from Sigma-Aldrich (St. Louis, MO) unless otherwise indicated. Antibodies were purchased from Roche Diagnostic Corporation, Germany (sheep polyclonal antidigoxigenin anti-DIG, antidigoxigenin Fab fragments), Sigma-Aldrich, USA (mouse monoclonal anti-2,4-dinitrophenol anti-DNP), Bio-Rad, UK (mouse polyclonal anti-Salmonella), Zeptometrix Corporation, USA (murine monoclonal anti-p17, anti-HIV antibody). Anti-AT20 monoclonal antibody (MBS-3) was produced as previously described.[27] Polyclonal antibodies to the p17 AT20 epitope were produced by immunizing mice with KLH-conjugated AT20 peptide (AT20-KLH), as reported elsewhere.[28] All the antibodies were aliquoted in PBS pH 7.4 and stored at 4 °C for immediate use or at

DOI: 10.1021/jacs.7b09347
J. Am. Chem. Soc. XXXX, XXX, XXX−XXX

−20 °C for long-term storage. Bovine blood serum was purchased from Sigma-Aldrich and human blood plasma samples were collected from HIV-positive patients vaccinated or not with AT20-KLH.[29]

Oligonucleotides. All oligonucleotide employed in this work were synthesized, labeled, and purified (HPLC and reverse phase) by IBA GmbH (Göttingen, Germany) and used without further purification. Unless otherwise stated the labeled oligonucleotides were dissolved in Millipore water at a concentration of 1 mM while the nonlabeled oligonucleotides were dissolved in the relevant buffer at a concentration of 100 μM. The final concentration of the oligonucleotides was confirmed using Tecan Infinite M200pro (Männedorf, Switzerland) through NanoQuant Plate. The sequences of the oligonucleotides used were as follows. Strand #1 of the sensing platform (DNA-based stem-loop) was terminally modified with AF488 (AlexaFluor488) or AF555 (AlexaFluor555) or AF680 (AlexaFluor680) and internally with BHQ-1 (black hole quencher 1) or BHQ-2 (black hole quencher 2) as noted below. Internal modifications were linked to these oligonucleotides via the C5-position of the appropriate thymine base. PNA/Peptide chimera probes were purchased from Panagene, South Korea. The sequences and modification schemes of the oligonucleotide sequences are as follows.

(1) **Anti-DNP targeting nanoswitches**

Strand #1:

5′-(AF555)-T **GAGCG** GTA TAG CCT AAT TCG **CGCTC** T (BHQ2) CTG TCA CTT TCT GAG-3′.

DNP-modified strand #2:

5′-DNP-*TTT TT* CTC AGA AAG TGA CAG-3′.

DNP-modified input strand (strand #3) (16-mer):

5′-DNP-*TTT TTT TTT TTT TTT* CGA ATT AGG CTA TAC C-3′.

DNP-modified input strand (strand #3) (15-mer):

5′-DNP-*TTT TTT TTT TTT TTT* CGA ATT AGG CTA TAC-3′.

DNP-modified input strand (strand #3) (14-mer):

5′-DNP-*TTT TTT TTT TTT TTT* CGA ATT AGG CTA TA-3′.

DNP-modified input strand (strand #3) (13-mer):

5′-DNP-*TTT TTT TTT TTT TTT* CGA ATT AGG CTA T-3′.

(2) **Anti-DIG targeting nanoswitches**

DIG strand #1:

5′-(AF488)-T **AGG CG** TTC TAG ATA TGC AAT **CGC CT** T (BHQ1) GTC TCA GAA TGT AAG-3′.

DIG-modified strand #2:

5′-DIG-*TTT TT* CTT ACA TTC TGA GAC-3′.

DIG-modified input strand (strand #3):

5′-DIG-*TTT TTT TTT TTT TTT* ATT GCA TAT CTA GAA-3′.

(3) **Anti-p17 targeting nanoswitches**

p17 strand #1:

5′-(AF680)-T **ACG TG** ATC TAA TGG TGA GTC **CAC GT** T (BHQ2) CTA GAA TAA AAC GCC ACT G-3′.

p17-modified strand #2 (PNA-Peptide chimera probe):

N_{term}-<u>ELDRWEKIRLRP</u>-CAG TGG CGT TTT ATT CT-C_{term}.

p17-input strand (strand #3): 5′-GAC TCA CCA TTA GAT A TTT TTT TTT TTT TTT TTT TTT TTT TT CTT AGA ATA AAA CGC CAC TG-3′.

(4) **Anti-AT20 targeting nanoswitches**

AT20 strand #1:

5′-(AF680)-T **ACG TG** ATC TAA TGG TGA GTC **CAC GT** T (BHQ2) CTA GAA TAA AAC GCC ACT G-3′.

AT20-modified strand #2 (PNA-Peptide chimera probe):

N_{term}-<u>SGGELDRWEKIRLRPGGKKK</u>-CAG TGG CGT TTT ATT-C_{term}.

AT20-input strand (strand #3): 5′-GAC TCA CCA TTA GAT A TTT TTT TTT TTT TTT TTT TTT TTT TT CTT AGA ATA AAA CGC CAC TG-3′.

In the above sequences the italic bases denote the poly thymine tails and linkers introduced to enhance flexibility of the system. Underlined bases represent peptide portion (p17 and AT20 peptide) that are terminally conjugated to PNA (PNA-Peptide chimera). In bold are reported the five bases of the stem of the DNA-based nanoswitches.

Fluorescence Experiments. All DNA oligos were stored (100 μM) and used in a 100 mM TRIS buffer, pH 8. Fluorescence experiments were conducted at pH 7.0 in 50 mM Na_2HPO_4 buffer, 150 mM NaCl in a 100 μL cuvette. Equilibrium fluorescence measurements were obtained using a Cary Eclipse Fluorimeter respectively with excitation at 480 (±5) nm (for DNA nanoswitches labeled with FAM) and acquisition at 517 (±5) nm, with excitation at 555 (±5) nm (for DNA nanoswitches labeled with AF555) and acquisition at 575 nm and with excitation at 680 (±5) nm (for DNA-switches labeled with AF680) and acquisition at 702 (±5) nm. Binding curves reported in Figure 2 were obtained using 10 nM of the DNP strand #1 and DNP-modified strand #2 by sequentially increasing the concentration of the DNP-modified input strand (strand #3) in the absence and presence of anti-DNP antibodies (i.e., 100 nM). Binding curves reported in Figure 3 were obtained using 10 nM of the DNP strand #1, DNP-modified strand #2 and DNP-modified input strand and by sequentially increasing the concentration of anti-DNP antibodies. Binding curves reported in Figures 4 and 6 were achieved using 20 nM of p17/AT20 strand #1 and p17/AT20-input strand (strand #3) in the presence of 40 nM of p17/AT20-modified strand #2. For each concentration the fluorescence signal was recorded every 10 min until it reached equilibrium. To monitor the immune response of patients under HIV-vaccine treatments, 90 μL of Na_2HPO_4 (50 mM) and NaCl (150 mM) at pH 7.0 containing the AT20-reporter and input modules (strand #1, 20 nM; strand #2, 40 nM; strand #3, 20 nM) were added to 10 μL of blood plasma sample and the fluorescence signal measured after 10 min. Binding curves were obtained by plotting signal gain % (SG%) vs concentration of target (i.e., antibody) in solution, and fitting the data with the following simplified Langmuir-type equation:

$$\%\text{Signal Gain} = B \times \frac{[\text{Target}]}{K_{1/2} + [\text{Target}]}$$

where A is the fluorescence background, B is the maximum signal gain ($SG\%_{max}$) and $K_{1/2}$ is the concentration of target at half-maximum signal gain. Signal Gain % is calculated from the enhancement of fluorescence intensity achieved upon the addition of the antibody, relatively to the initial signal with the strand #1, #2 and #3 mixture using the following formula:

$$\%\text{Signal Gain} = \frac{[I_{Fluo}(T) - I_{Fluo}(0)]}{I_{Fluo}(0)} \times 100$$

where $I_{Fluo}(T)$ is the fluorescence signal obtained in the presence of the target antibody and $I_{Fluo}(0)$ is the fluorescence signal obtained in the absence of the target. To allow for more ready interpretation of the results, fluorescence signal obtained have been normalized on a 0−1 scale using the following formula:

$$\text{Rel. Fluor.} = \frac{[I_{Fluo}(T) - I_{Fluo}(0)]}{I_{Fluo}(\max) - I_{Fluo}(0)} \times 100$$

where $I_{Fluo}(\max)$ represents the maximum fluorescence signal of the platform related to saturating concentration of the target (Rel. Fluor. = 1), whereas $I(0)$ is the background signal (Rel. Fluor. = 0) and so the signal of the platform in the absence of the target.

ELISA Assays. Anti-AT20 specific antibodies in plasma samples obtained from patients vaccinated or not with AT20-KLH were also detected using a conventional ELISA.[29] Each well of 96-well microtiter plates (Maxisorp; Nunc, Roskilde, Denmark) was coated with 10 μg/mL of AT20 in 100 μL of carbonate/bicarbonate buffer, pH 9.6, overnight at room temperature. Wells were then saturated with 200 μL/well of PBS containing 2% bovine serum albumin (BSA) (wt/vol; assay buffer) for 1 h at 37 °C, and allowed to react with plasma diluted in assay buffer from 1:100 to 1:12.800 for 30 min at 37 °C. After

DOI: 10.1021/jacs.7b09347
J. Am. Chem. Soc. XXXX, XXX, XXX−XXX

washing 4 times with PBS containing 0.1% Tween-20 (vol/vol; washing buffer), the amount of bound antibody was determined by adding HRP-labeled goat antihuman or antimouse IgG.

■ ASSOCIATED CONTENT

Supporting Information

The Supporting Information is available free of charge on the ACS Publications website at DOI: 10.1021/jacs.7b09347.

Binding curves, control experiments and specificity tests for anti-DIG, anti-DNP and anti-HIV1 p17 antibodies detection, competitive fluorescence antibody-based detection of DNP in solution and comparison with ELISA method for Anti-AT20 antibodies detection (PDF)

■ AUTHOR INFORMATION

Corresponding Author

*francesco.ricci@uniroma2.it

ORCID

Francesco Ricci: 0000-0003-4941-8646

Author Contributions

#AP and RI contributed equally.

Notes

The authors declare no competing financial interest.

■ ACKNOWLEDGMENTS

This work was in part supported by Associazione Italiana per la Ricerca sul Cancro, AIRC (project no. 14420) (FR).

■ REFERENCES

(1) Cutts, J. C.; Powell, R.; Agius, P. A.; Beeson, J. G.; Simpson, J. A.; Fowkes, F. J. I. *BMC Med.* **2014**, *12*, 150−170.

(2) Gubala, V.; Harris, L. F.; Ricco, A. J.; Tan, M. X.; Williams, D. E. *Anal. Chem.* **2012**, *84*, 487−515.

(3) Gao, W.; Emaminejad, S.; Nyein, H. Y. Y.; Challa, S.; Chen, K.; Peck, A.; Fahad, H. M.; Ota, H.; Shiraki, H.; Kiriya, D.; Lien, D.-H.; Brooks, G. A.; Davis, R. W.; Javey, A. *Nature* **2016**, *529*, 509−514.

(4) Perfézou, M.; Turner, A.; Merkoçi. *Chem. Soc. Rev.* **2012**, *41*, 2606−2622.

(5) Nunes Pauli, G. E.; De La Escosura-Muñiz, A.; Parolo, C.; Helmuth Bechtold, I.; Merkoçi, A. *Lab Chip* **2017**, *15*, 399−405.

(6) Engelen, W.; Meijer, L. H. H.; Somers, B.; De Greef, T. F. A.; Merkx, M. *Nat. Commun.* **2017**, *8*, 14473−14481.

(7) Janssen, B. M. G.; Van Rosmalen, M.; Van Beek, L.; Merkx, M. *Angew. Chem., Int. Ed.* **2015**, *54*, 2530−2533.

(8) Tian, L.; Heyduk, T. *Anal. Chem.* **2009**, *81*, 1147−1156.

(9) Heyduk, E.; Dummit, B.; Chang, Y.-H.; Heyduk, T. *Anal. Chem.* **2008**, *80*, 5152−5159.

(10) Geddie, M. L.; Matsumura, I. *J. Mol. Biol.* **2007**, *369*, 1052−1059.

(11) Banala, S.; Aper, S. J. A.; Schalk, W.; Merkx, M. *ACS Chem. Biol.* **2013**, *8*, 2127−2132.

(12) Arts, R.; Den Hartog, I.; Zijlema, S. E.; Thijssen, V.; Van Der Beelen, S. H. E.; Merkx, M. *Anal. Chem.* **2016**, *88*, 4525−4532.

(13) Mahshid, S. S.; Camiré, S.; Ricci, F.; Vallée-Bélisle, A. *J. Am. Chem. Soc.* **2015**, *137*, 15596−15599.

(14) White, R. J.; Kallewaard, H. M.; Hsieh, W.; Patterson, A. S.; Kasehagen, J. B.; Cash, K. J.; Uzawa, T.; Soh, H. T.; Plaxco, K. W. *Anal. Chem.* **2012**, *84*, 1098−1103.

(15) Vallée-Bélisle, A.; Ricci, F.; Uzawa, T.; Xia, F.; Plaxco, K. W. *J. Am. Chem. Soc.* **2012**, *134*, 15197−15200.

(16) Plaxco, K. W.; Cash, K. J.; Ricci, F. *J. Am. Chem. Soc.* **2009**, *131*, 6955−6957.

(17) Lubin, A. A.; Plaxco, K. W. *Acc. Chem. Res.* **2010**, *43*, 496−505.

(18) Zhang, Z.; Hejesen, C.; Kjelstrup, M. B.; Birkedal, V.; Gothelf, K. V. *J. Am. Chem. Soc.* **2014**, *136*, 11115−11120.

(19) Ranallo, S.; Rossetti, M.; Plaxco, K. W.; Vallée-Bélisle, A.; Ricci, F. *Angew. Chem., Int. Ed.* **2015**, *54*, 13214−13218.

(20) Lu, K.; Duan, Q. P.; Ma, Li; Zhao, D. *Bioconjugate Chem.* **2010**, *21*, 187−202.

(21) Trads, J. B.; Tørring, T.; Gothelf, K. V. *Acc. Chem. Res.* **2017**, *50*, 1367−1374.

(22) Rosier, B. J. H. M.; Cremers, G. A. O.; Engelen, W.; Merkx, M.; Brunsveld, L.; De Greef, T. F. A. *Chem. Commun.* **2017**, *53*, 7393−7396.

(23) Singhal, A.; Bagnacani, V.; Corradini, R.; Nielsen, P. E. *ACS Chem. Biol.* **2014**, *9*, 2612−2620.

(24) De Gregorio, E.; Rappuoli, R. *Nat. Rev. Immunol.* **2014**, *14*, 505−514.

(25) Jones, L. H. *Nat. Chem.* **2015**, *7*, 952−960.

(26) Iaria, M. L.; Fiorentini, S.; Focà, E.; Zicari, S.; Giagulli, C.; Caccuri, F.; Francisci, D.; Di Perri, G.; Castelli, F.; Baldelli, F.; Caruso, A. *Vaccine* **2014**, *32*, 1072−1078.

(27) Fiorentini, S.; Marsico, S.; Becker, P. D.; Iaria, M. L.; Bruno, R.; Guzmán, C. A.; Caruso, A. *Vaccine* **2008**, *26*, 4758−4865.

(28) Fiorentini, S.; Giagulli, C.; Caccuri, F.; Magiera, A. K.; Caruso, A. *Pharmacol. Ther.* **2010**, *128*, 433−444.

(29) Foca, E.; Iaria, M. L.; Caccuri, F.; Fiorentini, S.; Motta, D.; Giagulli, C.; Castelli, F.; Caruso, A. *HIV Clin. Trials* **2015**, *16*, 157−162.

DOI: 10.1021/jacs.7b09347
J. Am. Chem. Soc. XXXX, XXX, XXX−XXX

Supporting Information:

Programmable nucleic acid nanoswitches for the rapid, single-step detection of antibodies in bodily fluids

Alessandro Porchetta[1, #], Rudy Ippodrino[2, #], Bruna Marini[2], Arnaldo Caruso[3], Francesca Caccuri[3] and Francesco Ricci[1,*]

[1] *Department of Chemistry, University of Rome, Tor Vergata, Via della Ricerca Scientifica, 00133, Rome, Italy;*

[2] *Ulisse BioMed S.r.l., Area Science Park, 34149, Trieste, Italy;*

[3] *University of Brescia Medical School, Dept. of Molecular and Translational Medicine, Section of Microbiology, Piazzale Spedali Civili 1, 25123 Brescia, Italy;*

# These authors contributed equally to this work.

* Corresponding author: francesco.ricci@uniroma2.it

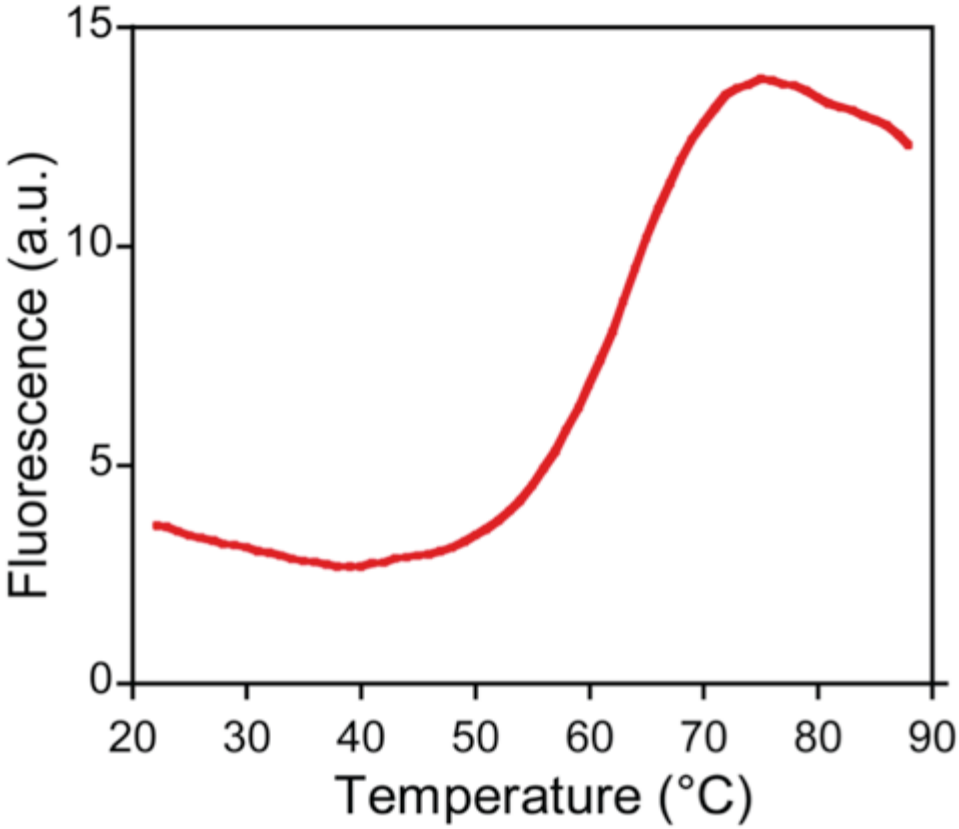

Figure SI1. Melting curve of the DNP-modified strand #1 shows that stem-loop is highly stable in the range of temperatures of interest for clinical applications (from 25 to 35 °C). The melting curve in this figure was performed in 50 mM Na_2HPO_4 and 150 mM NaCl at pH 7.0, with the DNP-modified strand #1 concentration of 100 nM.

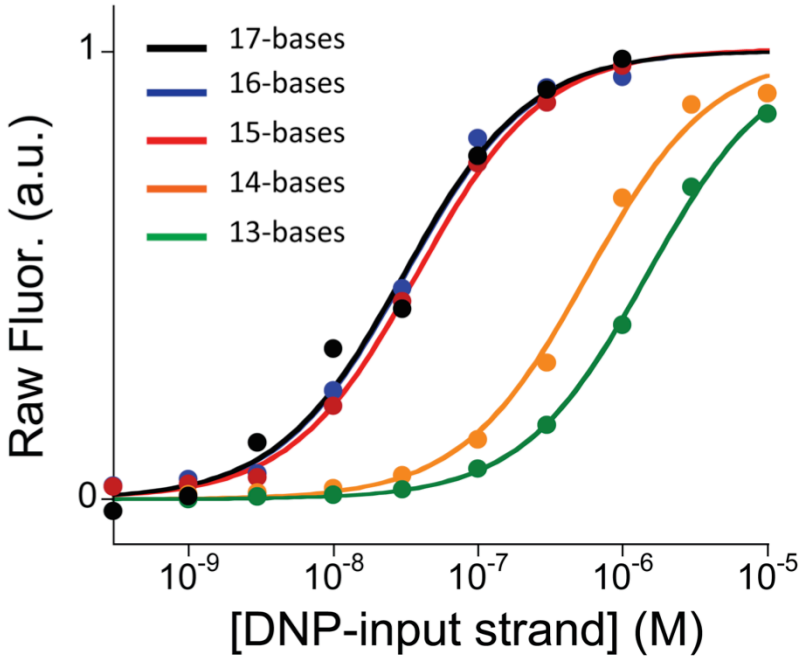

Figure SI2. Binding curves obtained with the DNP-reporter module (DNP strand #1 + DNP-modified strand #2) with increasing concentrations of DNA-input strand (strand #3) of different length (from 13 to 17 bases) in the absence of the anti-DNP antibody. Here the DNP-reporter module concentration is 10 nM (equimolar concentration of DNP strand #1 and DNP-modified strand #2). These and the following SI experiments were obtained at 35°C in 100 µL solution of Na_2HPO_4 (50 mM) and NaCl (150 mM) at pH 7.0, unless otherwise stated.

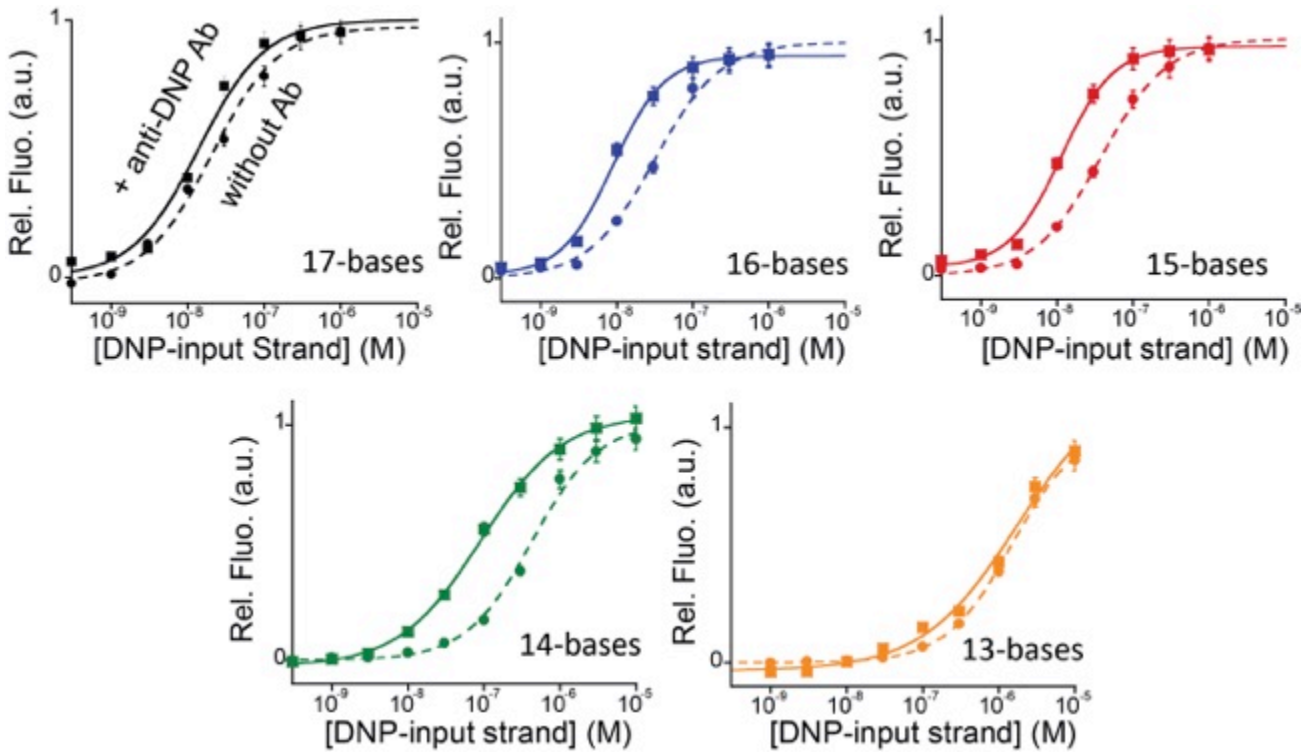

Figure SI3. Binding curves between the DNP-reporter module and DNA-input strand of different length (from 13 to 17 bases) in the absence and presence of the anti-DNP antibody (i.e. 100 nM). The presence of the anti-DNP antibodies causes an improvement of the binding affinity compared with the binding affinity reported in absence of anti-DNP antibody. Binding curves here were obtained using 10 nM of the DNP strand #1 and DNP-modified strand #2 by sequentially increasing the concentration of the DNP-modified input strand (strand #3) in the absence and presence of anti-DNP antibodies (i.e. 100 nM).

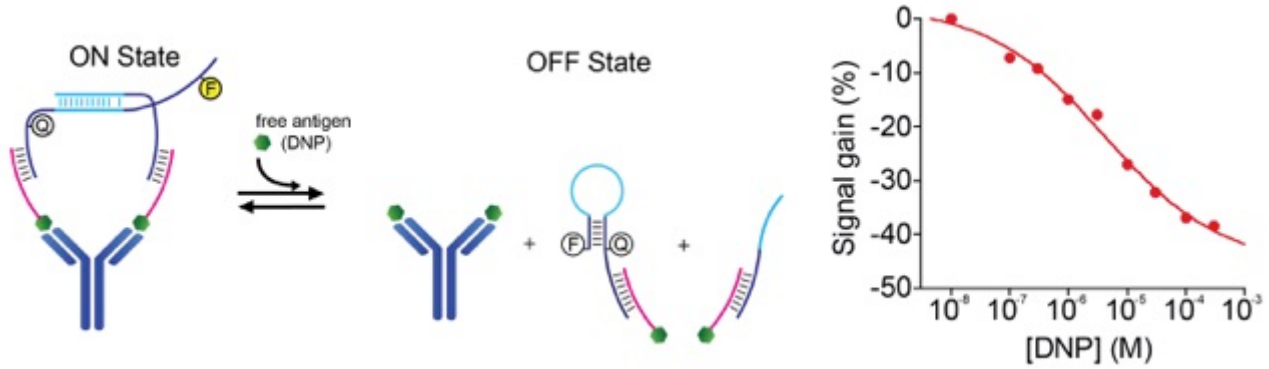

Figure SI4. Competitive fluorescence antibody-based detection of DNP in solution. The experiment is obtained using the DNP-reporter module (equimolar concentration of DNP strand #1 and DNP-modified strand #2, 10 nM) and the DNP-input strand at 10 nM in the presence of 10 nM anti-DNP antibody, and by sequentially increasing the concentration of free DNP in solution.

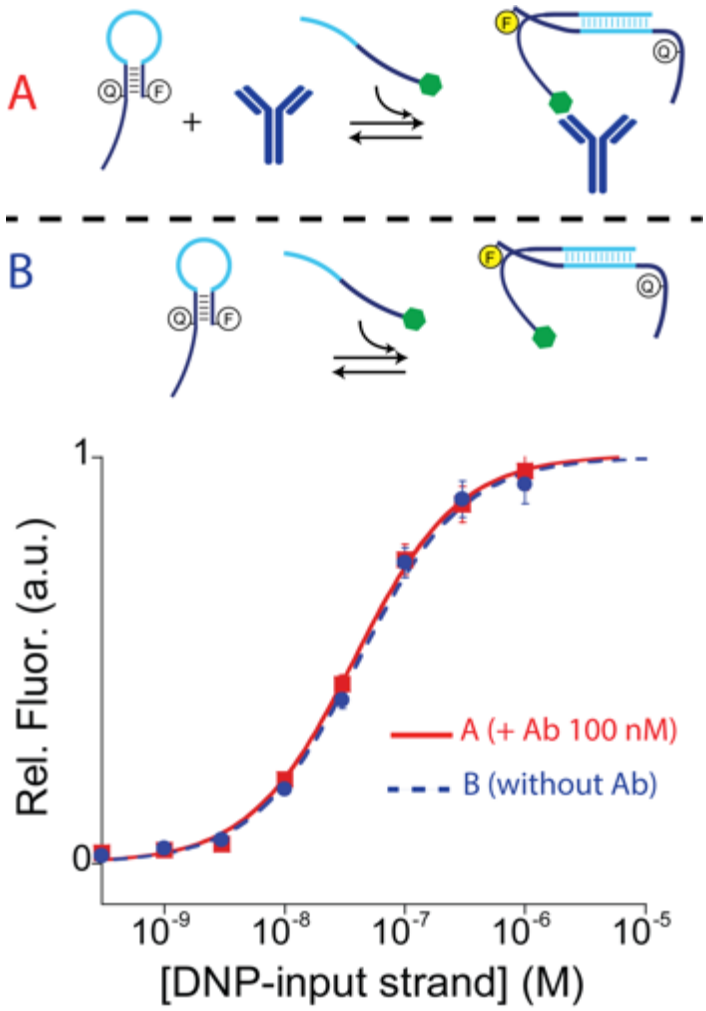

Figure SI5. Binding curves at increasing concentration of DNP-input strand in the absence of DNP-modified strand #2. Here binding curves were obtained using 10 nM of the DNP-modified strand #1 in the presence (red curve) and in the absence (blue dashed curve) of 100 nM Anti-DNP antibody by sequentially increasing the concentration of DNP-input strand in solution. The two binding curves do not show any significant difference of the binding affinity thus confirming that the presence of DNP-modified strand #2 is necessary to support the proposed sensing mechanism.

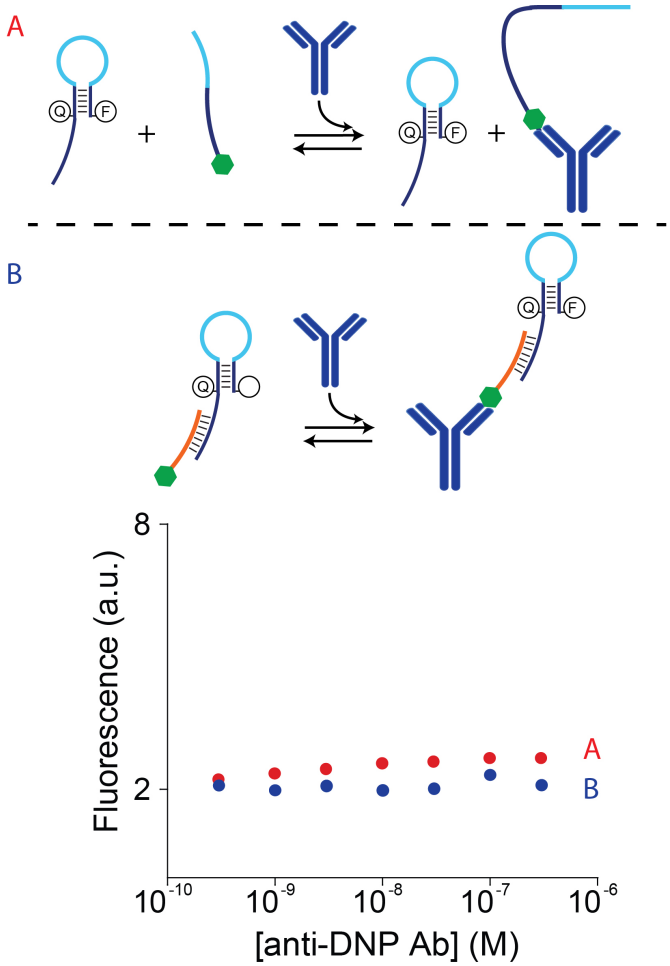

Figure SI6. Binding curve at increasing concentration of anti-DNP antibodies in the absence of DNP-modified strand #2 (A) and in the absence of strand #3 (B). Here binding curves were obtained using 10 nM of the DNP-modified strand #1 and 10 nM of strand#3 (A) or strand#2 (B) by sequentially increasing the concentration of anti-DNP antibodies in solution.

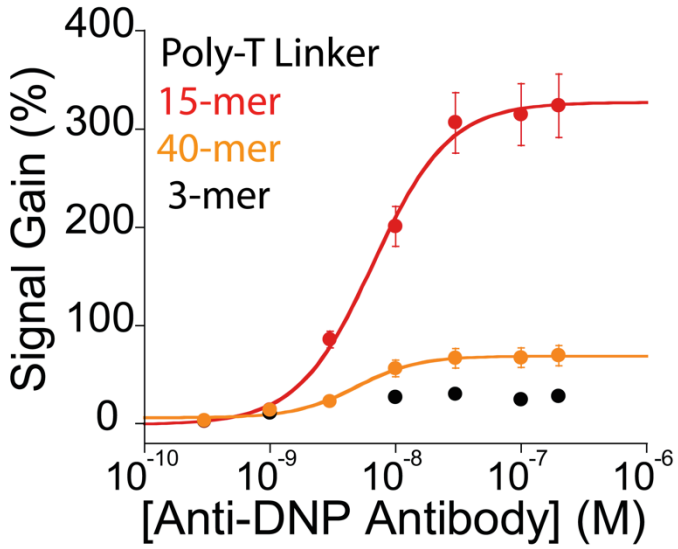

Figure SI7. Binding curve at increasing concentration of Anti-DNP antibodies using DNP-input strands contiaining the linker portion of different lengths (poly-thymine of 3, 15 and 40 bases). Here binding curves were obtained using 10 nM of the DNP-reporter module (equimolar concentration of DNP-modified strand #1 + DNP-modified strand #2, 10 nM) and 10 nM of the DNP-input strand (strand#3) by sequentially increasing the concentration of anti-DNP antibodies (i.e. 100 nM) in solution.

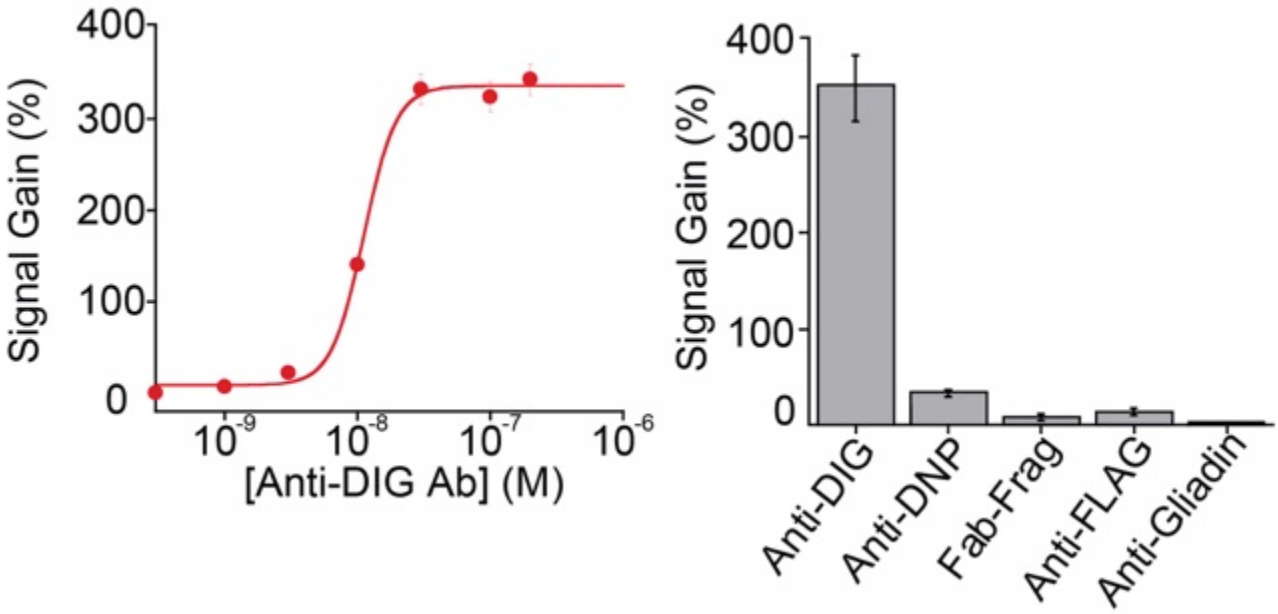

Figure SI8. Binding curve at increasing concentration of anti-Dig antibodies (left) and specificity test (right) using the Dig-reporter module. Here binding curves were obtained using 10 nM of the DIG-reporter module (equimolar concentration of DIG strand #1 + DIG-modified strand #2, 10 nM) and 10 nM of the DIG-input strand (strand#3) by sequentially increasing the concentration of anti-DIG antibodies (i.e. 100 nM) in solution. Specificity test were performed using 100 nM of non-specific antibodies.

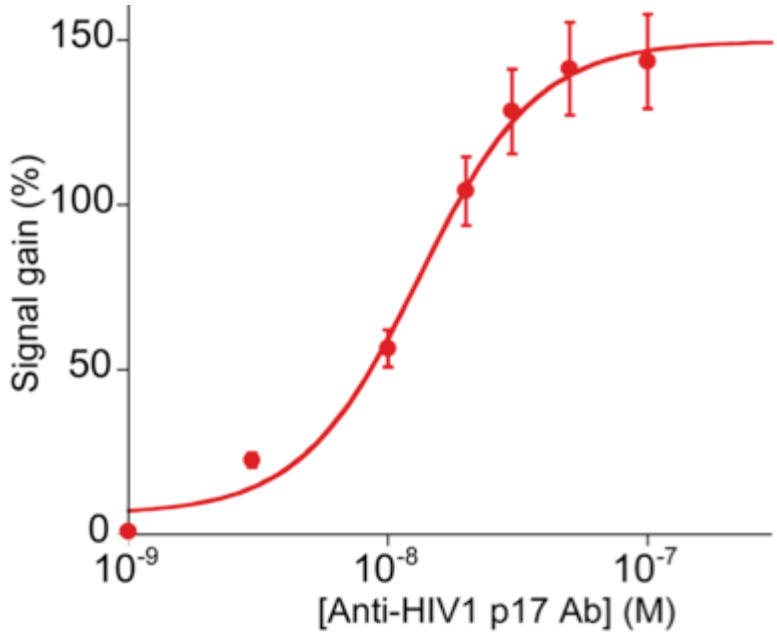

Figure SI9. Binding curve for anti-HIV1 p17 antibodies of the HIV-responsive module (anti-p17) in a solution of 90% bovine serum and 10% buffer (50 mM Na_2HPO_4 and 150 mM NaCl at pH 7.0). The binding curves were recorded using the HIV-reporter module concentration (equimolar concentration of p17 strand #1 and p17-modified strand #2, 20 nM) and the HIV-input module (equimolar concentration of p17-modified strand #2 and p17-input strand, 20 nM) at the concentration of 20 nM.

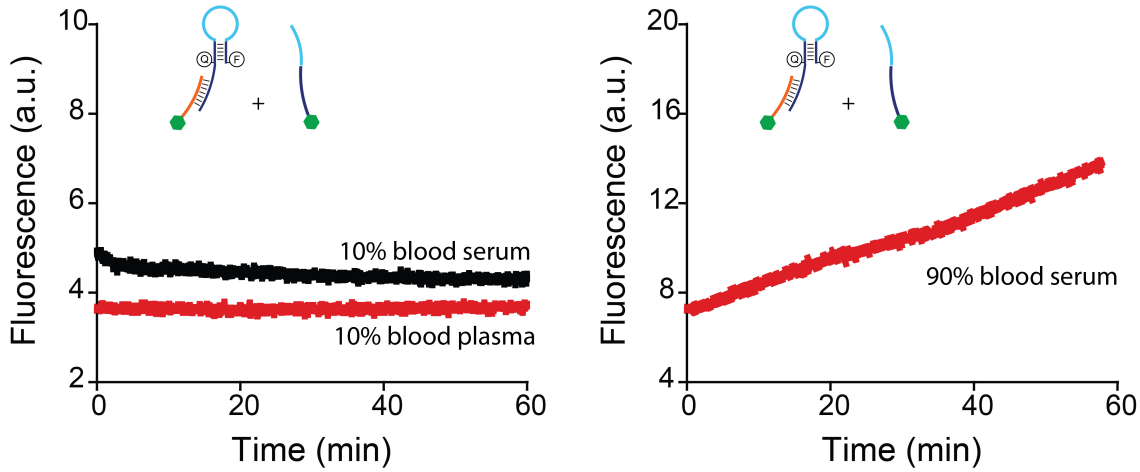

Figure SI10. The DNA nanoswitches are stable in human blood plasma (10%) and human serum (10%) over the course of the experiment. To demonstrate this we have employed the nanoswtiches for Anti-AT20 antibodies detection and measured continuously the fluorescence signal over a 60-minute period. No significant signal change was observed demonstrating that the degradation of the switches is minimal (left). A similar experiment was performed in a more complex matrix (90% serum) and we found that indeed the presence of nuclease in this matrix might lead to DNA degradation after a prolonged time (right). However, also in this case we note that over the time scale of our measurements (5-10 minutes) the signal drift observed is quite limited (0.1 a.u./min). (left) Kinetic fluorescence experiments were carried out at 35°C in a 100 µL solution obtained by mixing 10 µL of blank blood plasma (red) or blood serum (black) with 90 µL of Na_2HPO_4 (50 mM) and NaCl (150 mM) at pH 7.0 containing the AT20-reporter and input modules (strand #1, 20 nM; strand #2, 40 nM; strand #3, 20 nM). (right) Kinetic fluorescence experiments were carried out at 35°C in a 100 µL solution obtained by mixing 90 µL of blank blood serum with 10 µL of Na_2HPO_4 (50 mM) and NaCl (150 mM) at pH 7.0 containing the AT20-reporter and input modules (strand #1, 20 nM; strand #2, 40 nM; strand #3, 20 nM).

Antibody	Epitope
Anti-HIV1 p17 Ab	ELDRWEKIRLRP
Anti-AT20 MBS-3	SGGELDELDRWEKIRLRPGGKKK
Anti-MBS34	TKEALDKIEEEQNKSKKKAQQAAA

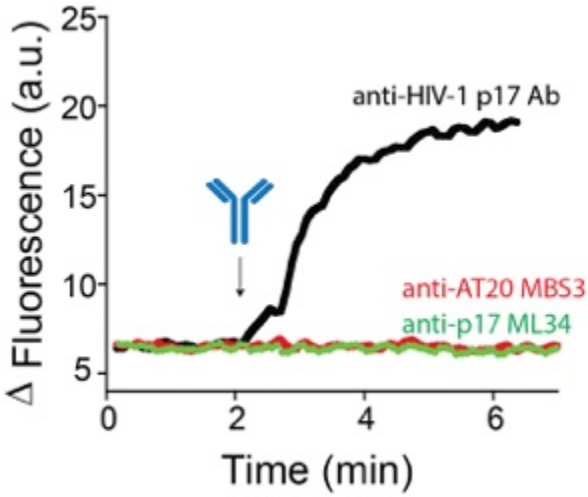

Figure SI11. The modular sensing platform for the detection of anti-HIV-1 p17 antibodies employing the p17 epitope as recognition element (orange sequence in the table) is able to detect anti-HIV-1 p17 antibodies in less than five minutes. No signal change is observed in the presence of anti-AT20 and anti- MBS-34 antibodies using this responsive module.

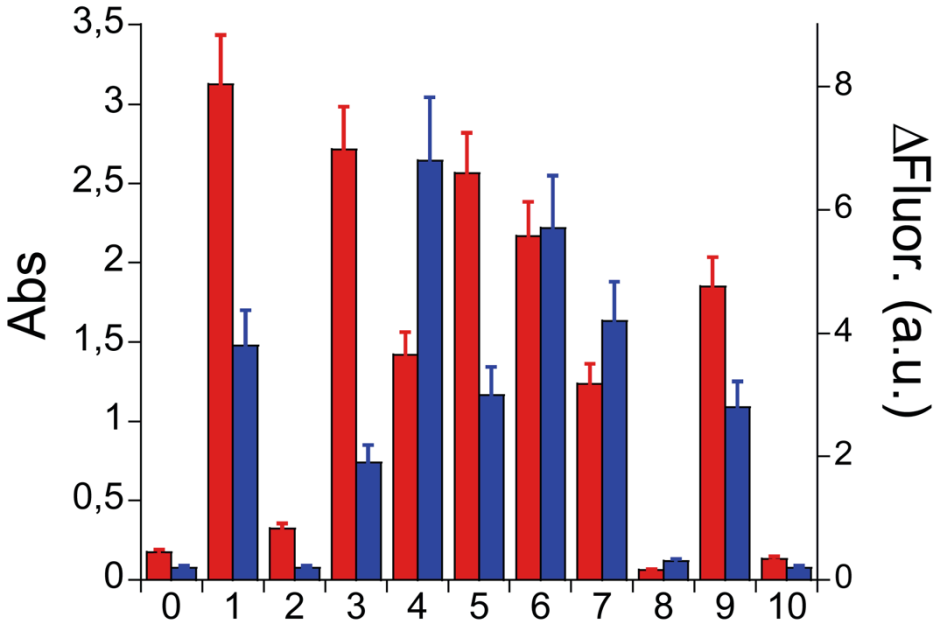

Figure SI12. Reactivity of plasma was tested against AT20 by solid-phase Enzyme-Linked Immunosorbent Assay (ELISA) (red bars, left y-axis). Here 1:400 dilution of plasma was used to perform titration in a solid-phase peptide ELISA assay. Each plasma pool was run in ELISA assays in triplicate. Threshold value was calculated to be 0.48, three standard deviation (SD) intervals from the mean values of three blank samples of HIV-negative patients. As a comparison the values obtained with the DNA nanoswitches are also shown here (blue bars, right y-axis)